Maintenance of long-term transposable element activity in genomes through regulation by nonautonomous elements

Adekanmi Daniel Omole[1], Peter Czuppon[1]

[1]Institute for Evolution and Biodiversity, University of Münster, Germany

Abstract

Transposable elements are DNA sequences that can move and replicate within genomes. Broadly speaking, two element types exist: autonomous elements, which encode the necessary enzymes for transposition, and nonautonomous elements that rely on these enzymes produced by autonomous elements for their transposition. Nonautonomous elements have been proposed to regulate transposable element numbers, which is a possible explanation for continued transposition activity over long evolutionary times. However, previous modeling studies indicate that interactions between autonomous and nonautonomous elements usually result in the extinction of one type. Here, we study a stochastic model that allows for stable coexistence of autonomous and nonautonomous elements. We determine the conditions for coexistence and derive an analytical expression for the stationary distribution of their copy numbers, showing that nonautonomous elements regulate stochastic fluctuations and the number of autonomous elements in stationarity. We find that the stationary variances of each element can be expressed as a function of transposable element copy number averages and their covariance, enabling data comparison and model validation. These results suggest that besides silencing or domestication of transposable elements, continued regulated transposition by nonautonomous elements may be an alternative evolutionary outcome that could for example explain the long co-evolutionary history of autonomous *LINE1* and nonautonomous *Alu* element transposition in the human ancestry.

Keywords: host silencing, trap model, genome evolution, genetics, linear noise approximation, stochastic model, essential public good.

1 Introduction

Transposable elements (TEs) are mobile genetic elements that relocate and replicate in genomes of species across the entire tree of life, from bacteria to animals and plants (Bennett, 2008; Hancks and Kazazian, 2012; Bennetzen and Wang, 2014). They constitute a substantial fraction of eukaryotic genomes, representing 45% of the human genome, over half of the genome in maize and zebrafish, and about one-third in *Drosophila melanogaster* and *Caenorhabditis elegans* (Cosby et al., 2019; Hayward and Gilbert, 2022). Far from being mere remnants of evolutionary history, TEs due to their ability to move, actively shape genomes and may even serve as catalysts of genetic innovations, contributing to the diversification of genes and genomes (Kazazian, 2004).

Nevertheless, TEs are regarded as genomic parasites because they pose potential threats to genomic integrity (Doolittle and Sapienza, 1980) and are sometimes labeled "selfish" due to their proliferation, which may not benefit the host organism and can be deleterious, potentially leading to genomic instability (Orgel and Crick, 1980; Bhat et al., 2022). This instability can arise from insertions that may disrupt promoters and enhancers, ectopic recombination between interspersed sequences that could result in deleterious chromosomal rearrangements, TE insertions into coding regions disrupting their function, or deleterious effects from TE-encoded complexes or products such as RNA or proteins (Montgomery et al., 1991; Cooke et al., 2014; Tubio et al., 2014). Based on these characteristics,

a TE life-cycle in genomes has been proposed (Le Rouzic et al., 2007): after TE invasion and establishment, TEs proliferate in the host genome until they become silenced or domesticated by the host. In each outcome, domestication or silencing, TEs lose their transposition ability. Yet, examples of TEs exist that have maintained their transposition ability over millions of years. One of the most prominent examples are LINE1 (L1) and Alu elements in the human genome lineage (Kazazian, 2004).

Essentially, three different explanations for such continued TE activity have been proposed (Brookfield and Badge, 1997). The first mechanism is referred to as transposition-selection balance (e.g. Charlesworth and Charlesworth, 1983; Charlesworth, 1991). Due to the negative fitness effects of TEs on their host, individuals with large TE copy numbers are selectively disadvantageous and produce less offspring than hosts with fewer numbers of TEs. Therefore, transposition of TEs in the genome is balanced by selection against large TE copy numbers on the host level, thus resulting in stable TE copy numbers over time. The second regulation mechanism is TE self-regulation (e.g. Charlesworth and Charlesworth, 1983; Charlesworth and Langley, 1986). Here, the transposition rate of TEs decreases with TE copy number. This is reminiscent of ecological population models like logistic growth, the transposition rate corresponding to the growth rate and the TE copy number to the population size. This TE self-regulation will also result in stable copy numbers over time. The last regulation mechanism that has been suggested is based on an interaction between so called *autonomous* and *nonautonomous* TEs.

Autonomous TEs are encoding the entire transposition machinery necessary for their transposition. In contrast, non-autonomous TEs rely on the transposition machinery of autonomous elements, which is why they have been characterized in the literature as "hyperparasites" (Robillard et al., 2016), "superparasites" (Startek et al., 2013), and "parasites of parasites" (Suh, 2019). Examples of autonomous-nonautonomous TE pairs include the already mentioned L1 and Alu elements in the human genome (Boeke, 1997; Dewannieux et al., 2003; Wagstaff et al., 2012), RLG_*Wilma* and RLG_*Sabrina* in the wheat genome (Wicker et al., 2021), activator (Ac) and dissociation (Ds) elements in the maize genome (McClintock, 1956), or Tc1/mariner and *Stowaway* Miniature Inverted Repeat Transposable Elements (MITEs) in the rice genome (Feschotte et al., 2003). TEs are additionally characterized based on their transposition mechanism: copy-and-paste for RNA transposons or cut-and-paste transposition for DNA transposons. In this manuscript, we will focus on the former class of TEs, RNA transposons, also referred to as retrotransposons.

Various theoretical models have been developed to investigate the interactions between autonomous and nonautonomous retrotransposons. Interestingly, essentially all of these studies find that coexistence of nonautonomous and autonomous TEs is not possible over long periods of time (e.g. Brookfield, 1996; Le Rouzic and Capy, 2006; Startek et al., 2013). These studies usually model a nonautonomous TE as arising through mutations from the autonomous TE, making the two TE types related to each other, in the sense of sequence similarity. Moreover, all of these models assume deleterious fitness effects of TEs on the host. But even if the nonautonomous TE is 'unrelated' to the autonomous TE, a situation that was found to induce cyclic dynamics (Le Rouzic and Capy, 2006), no stable coexistence was found. A theoretical explanation for the continued transposition of for example the seemingly unrelated RLG_*Wilma* and RLG_*Sabrina* retrotransposon pair is therefore missing.

Here, we investigate this discrepancy between theoretical prediction and empirical observation. One detail that has not been considered explicitly in the previous studies are the molecular details of the interaction between the two TE types. To account for this, we explicitly model the molecular processes of transposition and study two 'unrelated' TE types, following the model by Xue and Goldenfeld (2016). TEs do not affect host fitness in this model. We study the stability of and stochastic fluctuations around the TE coexistence equilibrium. Importantly, our theoretical analysis provides a parameter-independent prediction about TE copy number variation in a host genome,

making it suitable for comparison with empirical data. Lastly, we investigate through simulations the potential regulatory role of nonautonomous TEs (Hartl et al., 1992; Brookfield and Badge, 1997). Concretely, we investigate if TE proliferation can be maintained even in the presence of host regulatory mechanisms. We model host regulation through the *trap model* (Kofler, 2019, 2020; Tomar et al., 2023), which is motivated by TE silencing through the piRNA pathway (Siomi et al., 2011; Czech and Hannon, 2016). In brief, piRNAs are small RNAs that specifically bind to Piwi proteins and TE transcripts, leading to either the degradation of these transcripts or the modification of the TE sequence through methylation. This effectively prevents TE transposition and through that contributes to the stability of the host genome (Brennecke et al., 2007).

We start by describing the model and analyzing the coexistence dynamics of the two TE types in a single lineage. Second, we explore how host regulation affects TE numbers in a host population.

2 Model

We study the dynamics of an autonomous-nonautonomous TE pair within a genome. We first describe the processes that are underlying the changes in TE copy number. We derive a pair of stochastic differential equations that model these dynamics. Last, we extend the model to include host regulation of TE dynamics. This requires a more detailed description of the host's genetic setup, specifically the components that interact with and regulate the TEs.

2.1 TE dynamics

The current mechanistic understanding of autonomous and nonautonomous retrotransposon mobilization can be summarized as follows (Dewannieux et al., 2003). When a protein encoded by an autonomous TE is synthesized at the ribosome, the autonomous transcript binds to the protein, likely recognizing its polyadenine (poly-A) tail, which it utilizes for retrotranscription into another genomic site, a phenomenon termed the *cis* replication (Wei et al., 2001). Meanwhile, nonautonomous transcripts co-localizing on the same ribosome can associate with the nascent protein encoded by the autonomous TE because of sequence-similarity of the poly-A tails of the two transcripts. The nonautonomous transcript associated is then retrotranscribed elsewhere in the genome, known as the *trans* replication (Boeke, 1997; Dewannieux et al., 2003). Motivated by this detailed description of the TE transposition process, we model the TE interaction as follows.

We denote the copy number of active autonomous and nonautonomous TEs within a genome at a given time t as $X(t)$ and $Y(t)$, respectively. Let C represent the complex of autonomous TE-encoded mRNA, cDNA, and nascent protein. An autonomous TE, X, encodes this complex at a rate a. Subsequently, the complex retrotransposes, producing a new X element at a rate b_1. Moreover, the complex C can serve as a template for a nonautonomous TE, Y, to replicate itself at a rate b_2. The number of (active) TEs decreases either by deactivation, e.g. through host silencing or mutations, or excision from the genome. We lump these degradation processes in the parameter d_1. TE-type specific degradation rates are investigated in Appendix C. Lastly, the complex undergoes degradation at a rate of d_2. These dynamics are illustrated in Fig. 1 and yield the following model, previously described by Xue and Goldenfeld (2016):

$$\begin{aligned} X &\xrightarrow{a} X + C, \qquad & C &\xrightarrow{b_1} X, \qquad & C + Y &\xrightarrow{b_2} 2Y, \\ X &\xrightarrow{d_1} \varnothing, & Y &\xrightarrow{d_1} \varnothing, & C &\xrightarrow{d_2} \varnothing\,. \end{aligned} \tag{1}$$

TE numbers in the germline change slowly from generation to generation in a host species population (Suh et al., 1995). Compared to this evolutionary time scale, the formation and degradation of the intermediate complex occur on a much faster time scale. Alternatively, TE numbers can

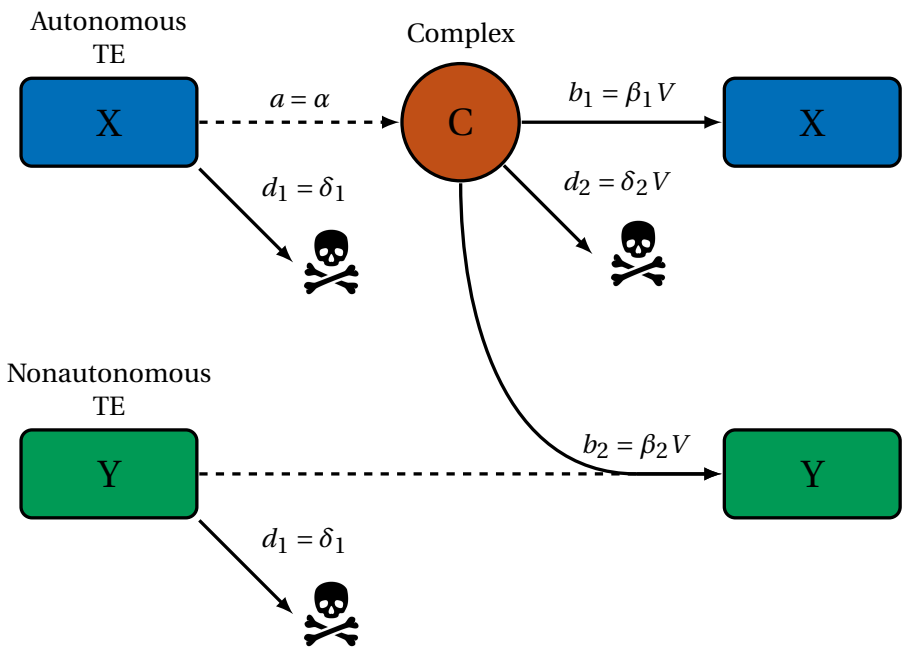

Figure 1: **Schematic of autonomous-nonautonomous TE interaction.** The diagrammatic description illustrates the interaction between autonomous and nonautonomous TEs. The autonomous TE, X, encodes the complex, C at a rate $a = \alpha$, and this complex retrotranscribes to produce a new X element at rate $b_1 = \beta_1 V$. The nonautonomous TE, Y, hijacks the complex produced by the autonomous TE to duplicate itself at the rate $b_2 = \beta_2 V$. Both types of TEs deactivate at rate $d_1 = \delta_1$, and the complex degrades at rate $d_2 = \delta_2 V$. Solid arrows indicate transformations that involve a change in numbers at the start and end of the arrow, dashed arrows indicate production, where only the numbers at the tip of the arrow change.

also change in the somatic cells, where the same distinction between fast complex and slow TE processes is appropriate. Mathematically, this translates to dynamics on two different time scales, which can be separated. To achieve this separation, we scale the number of TEs by the parameter V, which represents the order of magnitude of the number of TEs (or the length of the genome that the TEs occupy) and modeled to be much larger than the number of complexes. We then study the rescaled variables $x^V = X/V$ and $y^V = Y/V$ while the number of complexes remains on the original scale. Following classical mass action kinetics, we also transform the binary reaction rate b_2 by multiplying it with $1/V$, which now describes the probability of interaction between a complex and a nonautonomous TE; for a more detailed discussion of this classical scaling, we refer to Section 3.1 in Anderson and Kurtz (2011). To account for the relatively faster dynamics of the complex, we scale the rates as follows: $a = \alpha$, $b_1 = \beta_1 V$, $b_2 = \beta_2 V$, $d_1 = \delta_1$, $d_2 = \delta_2 V$. The scaling indicates that the formation of the complex at rate a and deactivation of the TEs at rate d_1 occur on the same (slow) time scale. Additionally, the scaling shows that once the complex is formed, the production of new autonomous and nonautonomous TEs at rates b_1 and b_2, respectively, occur on the same (fast) time scale as the degradation of the complex at rate d_2.

The stochastic dynamics of this rescaled system are then given by:

$$
\begin{aligned}
x^V(t) &= x^V(0) + \frac{1}{V} Y_2 \left(V \int_0^t \beta_1 C(s) ds \right) - \frac{1}{V} Y_4 \left(V \int_0^t \delta_1 x^V(s) ds \right) , \\
y^V(t) &= y^V(0) + \frac{1}{V} Y_3 \left(V \int_0^t \beta_2 C(s) y^V(s) ds \right) - \frac{1}{V} Y_5 \left(V \int_0^t \delta_1 y^V(s) ds \right) , \\
C(t) &= C(0) + Y_1 \left(V \int_0^t \alpha x^V(s) ds \right) - Y_2 \left(V \int_0^t \beta_1 C(s) ds \right) - Y_3 \left(V \int_0^t \beta_2 C(s) y^V(s) ds \right) \\
&\quad - Y_6 \left(V \int_0^t \delta_2 C(s) ds \right) ,
\end{aligned}
\tag{2}
$$

where $Y_i,\ i \in \{1, \ldots, 6\}$ are independent rate-1 Poisson processes corresponding to the reactions in Eq. (1).

For V sufficiently large, this system exhibits a time-scale separation, where the complex dynamics, $C(t)$, are occurring much faster than the dynamics of the two TE types, x^V and y^V. Consequently, given a certain TE configuration, the complex reaches a quasi-steady state (Ball et al., 2006). This equilibrium of the complex is given by

$$
C^* = \frac{\alpha x^V}{\beta_1 + \delta_2 + \beta_2 y^V} . \tag{3}
$$

To derive the stochastic differential equations (SDEs) corresponding to Eq. (2), we employ the infinitesimal generator and convergence results of density dependent Markov processes (Ethier and Kurtz, 1986, Chapters 4 & 11). We find

$$
\begin{aligned}
dx^V &= (\beta_1 C^* - \delta_1 x^V) dt + \sqrt{\frac{\beta_1 C^* + \delta_1 x^V}{V}} dW_t^x , \\
dy^V &= (\beta_2 C^* y^V - \delta_1 y^V) dt + \sqrt{\frac{\beta_1 C^* y^V + \delta_1 y^V}{V}} dW_t^y ,
\end{aligned}
\tag{4}
$$

where $(W_t^x)_{t \geq 0}$ and $(W_t^y)_{t \geq 0}$ are two independent standard Brownian motions, and the stochastic differential is interpreted in the sense of Itô. Inserting the equilibrium value of the complex gives

$$
\begin{aligned}
dx^V &= x^V \left(\frac{\beta_1 \alpha}{\beta_1 + \delta_2 + \beta_2 y^V} - \delta_1 \right) dt + \sqrt{\frac{x^V}{V} \left(\frac{\beta_1 \alpha}{\beta_1 + \delta_2 + \beta_2 y^V} + \delta_1 \right)} dW_t^x , \\
dy^V &= y^V \left(\frac{\beta_2 \alpha x^V}{\beta_1 + \delta_2 + \beta_2 y^V} - \delta_1 \right) dt + \sqrt{\frac{y^V}{V} \left(\frac{\beta_2 \alpha x^V}{\beta_1 + \delta_2 + \beta_2 y^V} + \delta_1 \right)} dW_t^y .
\end{aligned}
\tag{5}
$$

This system of stochastic differential equations is the basis of the subsequent analysis to derive our results.

2.2 Extension of the model to account for host silencing

In addition to the dynamics of TE copy numbers within a single genome, we investigate the interplay between the TE dynamics and potential host silencing. To this end, we model a population of N diploid individuals that reproduce according to Wright-Fisher dynamics (fixed population size and non-overlapping, discrete generations). We assume that TEs do not exert any fitness effect on their host, i.e., all hosts have the same chances to reproduce and dynamics are neutral. In our model, TE dynamics occur during the haploid stage of the life cycle, similar to the model by Kofler (2019). In detail, we have the following steps: (1) $2N$ gametes are chosen at random from the

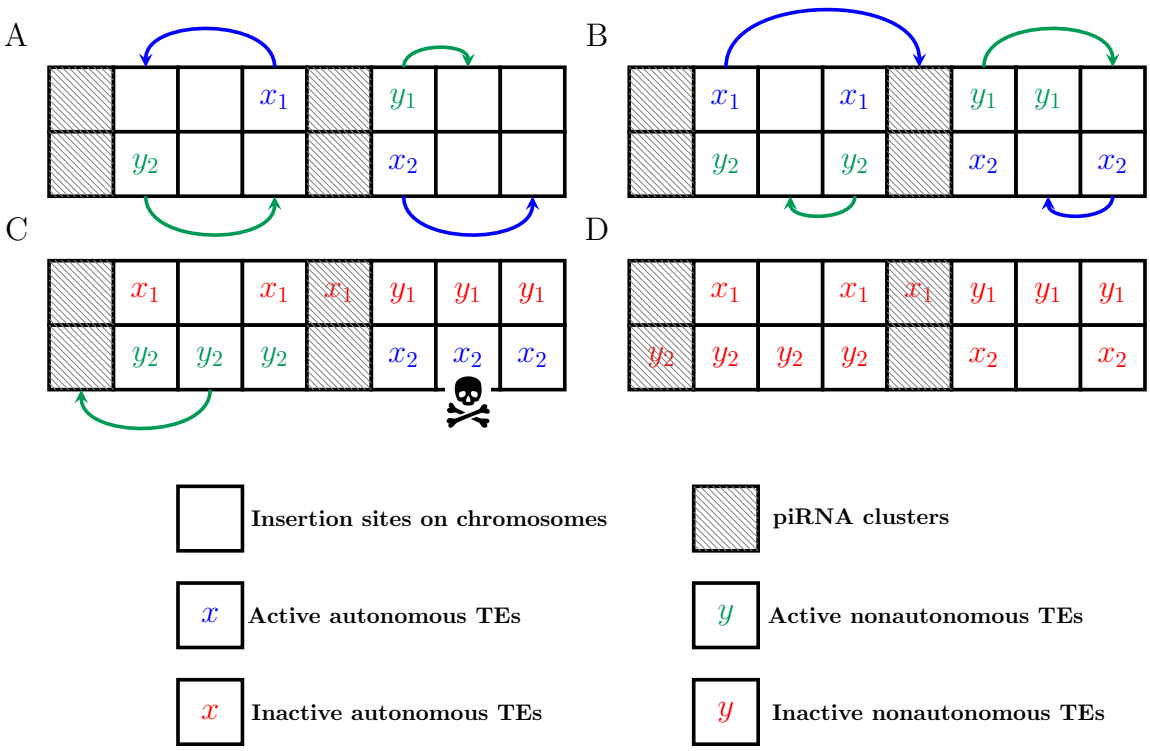

Figure 2: **Schematic representation of the trap model**. The two rows represent a diploid genome and potential TE insertion sites, which are symbolized by square boxes. Shaded regions describe the locations of piRNA clusters, the traps. The genome is populated with active autonomous (blue) and nonautonomous (green) TEs, denoted by x_i and y_i, respectively. The same genome is shown for four sequential generations (**A**–**D**). TEs can duplicate (arrows) or be deleted (skull). These processes continue until a TE copy, such as x_1 in **C**, jumps into the trap, where it becomes inactive (depicted in red), including all TEs integrated within the same haploid genome.

parental population, (2) TE dynamics occur on these haploid gametes, (3) two gametes are joined and identified as a diploid offspring individual. We ignore recombination in this model because we are not interested in the reshuffling of genomic material but simply in a potential silencing threshold level below which an actively transposing autonomous-nonautonomous TE pair can persist, which in fact reduces this model to a population of $2N$ haploid individuals.

Host silencing enters in step (2) of the life cycle and suppresses transposition of both autonomous and nonautonomous TEs. We model host silencing through the *trap model* (Kofler, 2019; Tomar et al., 2023), wherein TEs proliferate until at least one copy jumps into a piRNA cluster, referred to as the trap. This happens with a probability p, which we will also refer to as the silencing probability. It reflects the proportion of piRNA clusters in the host genome. Once a TE copy is located within a piRNA cluster, all TEs in the same haploid genome are silenced, i.e., their transposition is suppressed by the host (Fig. 2).

2.3 Stochastic simulations

We implemented the TE dynamics model (Eq. 1) using the standard stochastic simulation algorithm, also known as Gillespie's algorithm (Gillespie, 1976). For comparison, we also simulated the corresponding deterministic model for each TE type (deterministic part in Eq. (5)).

To simulate the trap model, we adapted the simulation as follows. First, we choose $2N$ haploid ga-

metes uniformly at random with replacement from all parental gametes. If TEs on the haploid genome are silenced nothing happens and TE numbers are carried over unchanged to the next generation. If TEs are not silenced, their dynamics are implemented by the Euler tau-leaping method (Gillespie, 2001): TE transposition and deletion events are drawn from a Poisson distribution where the rates are determined by the current TE numbers in the genome and the corresponding stationary number of complexes. To this end, rates are interpreted as 'per generation'.

Both simulations were executed in Julia, while all subsequent data analyses and plotting were performed in Python. The source codes and data files to reproduce the figures and simulation results are available at `https://github.com/Ade-omole/TEs_long_term`. Our default parameter set is stated in Table 1. We note that these parameters are much higher than what would be expected empirically. For example, α and δ_1 are estimated to be on the scale of $10^{-3} - 10^{-5}$ (Suh et al., 1995). However, this deviation from empirical evidence does not affect our general, parameter independent, results and speeds up simulations.

Parameter	Interpretation	Value
α	complex production rate	2.0
β_1	autonomous TE transposition rate	1.0
β_2	nonautonomous TE transposition rate	0.5
δ_1	TE deletion rate	0.5
δ_2	complex degradation rate	1.5
V	scaling parameter	500

Table 1: **Overview of parameters.** We summarize all parameter abbreviations, their biological interpretations and default values in the simulations.

3 Results

We now analyze the system of stochastic differential equations in Eq. (5) and numerically assess the validity and robustness of the theoretical analyses. We start by investigating the deterministic model, which exhibits a locally stable coexistence state with both autonomous and nonautonomous TEs under certain parameter configurations. We then study the stochastic dynamics and describe the stationary distribution by computing the fluctuations around the deterministic equilibrium. Lastly, we compare the theoretical prediction to stochastic simulations and study the effect of host silencing on TE copy numbers.

3.1 Stable coexistence of TE types

Deterministic equilibrium. The deterministic dynamics of the number of TEs from Eq. (5) are obtained by letting $V \to \infty$. For $x^V \to x$ and $y^V \to y$ we obtain

$$\begin{aligned} \frac{dx}{dt} &= x\left(\frac{\beta_1\alpha}{\beta_1+\delta_2+\beta_2 y} - \delta_1\right) = \mu_1(x,y)\,, \\ \frac{dy}{dt} &= y\left(\frac{\beta_2\alpha x}{\beta_1+\delta_2+\beta_2 y} - \delta_1\right) = \mu_2(x,y)\,. \end{aligned} \tag{6}$$

Setting both derivatives equal to zero, the equilibrium of system (6) is found as

$$(x^*, y^*) = \left(\frac{\beta_1}{\beta_2}, \frac{\beta_1\alpha - \delta_1\delta_2 - \beta_1\delta_1}{\beta_2\delta_1}\right)\,. \tag{7}$$

A non-trivial fixed point of the system, wherein both TE numbers are positive, exists if the parameters satisfy the following condition:

$$\beta_1\alpha - \delta_1\delta_2 - \beta_1\delta_1 > 0\,. \tag{8}$$

Local stability analysis. To analyze the local stability of the equilibrium described in Eq. (7), we compute the Jacobian matrix of the dynamics outlined in Eq. (6) at the equilibrium, given by

$$\mathbf{J}^* = \begin{pmatrix} \frac{\beta_1\alpha}{\beta_1+\delta_2+\beta_2 y^*} - \delta_1 & -\frac{x^*\beta_1\beta_2\alpha}{(\beta_1+\delta_2+\beta_2 y^*)^2} \\ \frac{\beta_2\alpha y^*}{\beta_1+\delta_2+\beta_2 y^*} & \frac{\beta_1\beta_2\alpha x^* + \beta_2\alpha\delta_2 x^*}{(\beta_1+\delta_2+\beta_2 y^*)^2} - \delta_1 \end{pmatrix} = \begin{pmatrix} 0 & -\frac{\delta_1^2}{\alpha} \\ \alpha - \delta_1 - \frac{\delta_1\delta_2}{\beta_1} & \delta_1\left(\frac{\delta_1(\beta_1+\delta_2)}{\beta_1\alpha} - 1\right) \end{pmatrix}. \tag{9}$$

Using the determinant-trace condition (e.g. Otto and Day, 2007, page 238), the eigenvalues of $\mathbf{J}^*$ have negative real part if $\det(\mathbf{J}^*) > 0$ and $\mathrm{tr}(\mathbf{J}^*) < 0$. Both conditions are satisfied if and only if the equilibrium is feasible, which is the case if Eq. (8) holds. Thus, the non-trivial equilibrium is locally stable if it exists.

To gain intuition about the condition for feasibility and local stability of the coexistence equilibrium, we rewrite condition (8) as follows:

$$\alpha \times \frac{1}{\delta_1} \times \frac{\beta_1}{\beta_1 + \delta_2} > 1\,. \tag{10}$$

The second term $(1/\delta_1)$ is the average life-time of an autonomous TE. Therefore, the first product α/δ_1 reflects the average number of produced complexes by a single autonomous TE until it is excised or becomes inactive. The last term (ratio $\beta_1/(\beta_1+\delta_2)$) is the probability that a complex produces an autonomous TE in the absence of nonautonomous TEs. Therefore, the left-hand side of Eq. (10) can be identified as the reproduction number of autonomous TEs in the absence of nonautonomous TEs. Interestingly, this implies that the coexistence of autonomous and nonautonomous TEs depends solely on the behaviour of the autonomous TEs. This is because condition (10) simplifies to $\beta_1\alpha/(\beta_1 + \delta_2) - \delta_1 > 0$, which is $\mu_1(x, 0)$ in Eq. (6). Therefore, coexistence of the two TEs is possible and (locally) stable if autonomous TEs grow exponentially in the absence of nonautonomous TEs.

The nonautonomous TE type plays a regulatory role in this interaction of the two TEs. This is apparent in Eq. (7), where β_2 scales the equilibrium TE copy number of the autonomous TE: the larger the rate of nonautonomous TE production, β_2, the smaller is the equilibrium value of the autonomous TE x^*. This implies that although the nonautonomous TE does not directly contribute to the stable coexistence of the two TEs through its own transposition, it plays a pivotal role in regulating TE proliferation.

Relative copy numbers of the TE types. The copy numbers of the two TE types rely on the interplay between the average number of complexes produced by the autonomous TEs and the average number of the complexes that are degraded before subsequent TE transposition. The conditions governing the relative copy numbers of the autonomous and nonautonomous TEs derived from Eq. (7) are as follows:

Proposition 1. *If the equilibrium is feasible (and therefore locally stable), then*

(a) $x^* < y^*$ *if and only if* $\frac{\alpha}{\delta_1} > 2 + \frac{\delta_2}{\beta_1}$,

(b) $x^* > y^*$ *if and only if* $1 < \frac{\alpha}{\delta_1} < 2 + \frac{\delta_2}{\beta_1}$,

(c) $x^* = y^*$ *if and only if* $\frac{\alpha}{\delta_1} = 2 + \frac{\delta_2}{\beta_1}$.

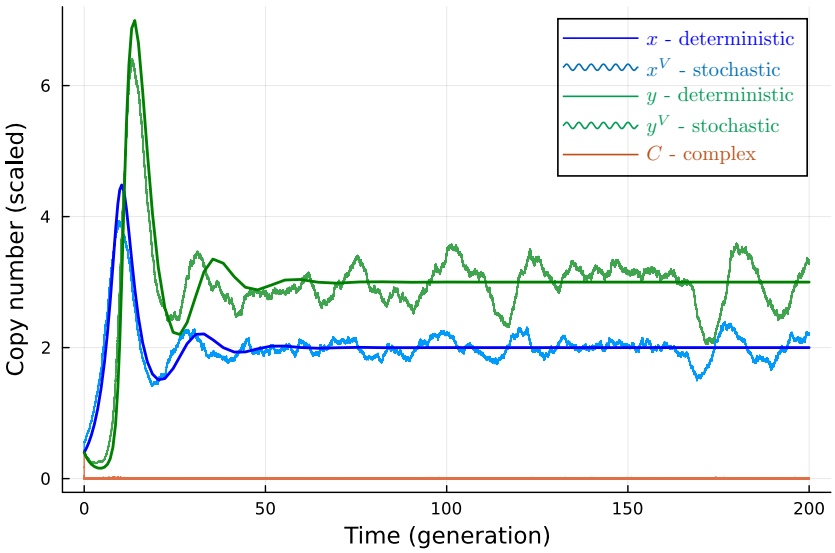

Figure 3: **Simulation of the autonomous-nonautonomous TE interaction.** The graph shows the deterministic (straight lines) and stochastic (wavy lines) dynamics of active autonomous (blue) and nonautonomous (green) TE copy numbers over time. The TEs approach their equilibrium in a cyclic way and then fluctuate around their respective equilibrium. In contrast, the complex (orange) quickly reaches its equilibrium and shows no visible fluctuations, visualizing the time scale separation. Parameter values are $\alpha = 2, \beta_1 = 1, \beta_2 = 0.5, \delta_1 = 0.5, \delta_2 = 1.5$, and $V = 500$.

The proof is stated in Appendix A.

The proposition provides additional insights into the relationship between the two types of TEs: The autonomous TE is more or less abundant than the nonautonomous TE depending on whether the average number of complexes produced by an autonomous TE before its deactivation, α/δ_1, is smaller or larger than the term $2 + \delta_2/\beta_1$. This term depends on the transposition rate of the autonomous TE but is independent of the nonautonomous transposition rate. If the transposition rate of the autonomous TE, β_1, is low, the term $2+\delta_2/\beta_1$ becomes large. This means that the average number of complexes required for the autonomous TE to be less abundant than the nonautonomous TE, as in (a), increases. Conversely, if the transposition rate of the autonomous TE, β_1, is high, the term $2+\delta_2/\beta_1$ approaches the value 2. This implies that the average number of complexes required for the autonomous TE to be less abundant is low, but above 2. This means that the parameter space for autonomous TEs to be less abundant than nonautonomous TEs decreases with decreasing autonomous transposition rate β_1, Fig. 7 in Appendix A. At the same time, the inverse conclusion holds true for the condition for autonomous TEs to be more abundant than nonautonomous TEs (part (b) of Proposition 1).

3.2 Stationary distribution of the TEs

We now examine the stochastic fluctuations of the stochastic process around the deterministic equilibrium. There are different approaches to study these fluctuations in systems with time-scale separations. The most accurate method involves deriving a central limit theorem for the stochastic process defined in Eq. (2) (Kang et al., 2014). Alternatively, a simpler approach is based on the Langevin equation (van Kampen, 2007), which uses the quasi-steady state assumption at every step, i.e., only the stationary number of complexes is taken into account. Here in the main text, we use the Langevin equation approach, also called the linear noise approximation. The analogous analysis

using the central limit theorem is relegated to Appendix D and yields almost the same result. The linear noise approximation derives the distribution of the process from the local dynamics around the deterministic equilibrium points through a Taylor expansion; we follow the exposition from Czuppon and Traulsen (2021). To this end, we study the fluctuations of two TE types around their respective equilibrium. The stochastic processes characterizing these fluctuations, denoted by U_1 and U_2, are defined as:

$$U_1(t) = \sqrt{V}(x^V(t) - x(t)), \qquad U_2(t) = \sqrt{V}(y^V(t) - y(t)), \tag{11}$$

where $x(t)$ and $y(t)$ represent the deterministic processes (Eq. (6)) associated to the stochastic processes $x^V(t)$ and $y^V(t)$ (Eq. (5)). Denoting $\mathbf{U} = (U_1, U_2)^\top$, the dynamics of the stochastic fluctuations can be approximated by

$$\begin{aligned}\frac{1}{\sqrt{V}}d\mathbf{U} &= \frac{1}{\sqrt{V}}\begin{pmatrix} dU_1 \\ dU_2 \end{pmatrix} = \frac{1}{\sqrt{V}}\begin{pmatrix} \mu_1(x^V, y^V) - \mu_1(x,y) \\ \mu_2(x^V, y^V) - \mu_2(x,y) \end{pmatrix} dt + \frac{1}{\sqrt{V}}\begin{pmatrix} \sqrt{x^V\left(\frac{\beta_1\alpha}{\beta_1+\delta_2+\beta_2 y^V} + \delta_1\right)}dW_t^x \\ \sqrt{y^V\left(\frac{\beta_2\alpha x^V}{\beta_1+\delta_2+\beta_2 y^V} + \delta_1\right)}dW_t^y \end{pmatrix} \\ &\approx \frac{1}{\sqrt{V}}\begin{pmatrix} \frac{\partial\mu_1}{\partial x} & \frac{\partial\mu_1}{\partial y} \\ \frac{\partial\mu_2}{\partial x} & \frac{\partial\mu_2}{\partial y} \end{pmatrix}\mathbf{U}dt + \frac{1}{\sqrt{V}}\begin{pmatrix} \sqrt{x^V\left(\frac{\beta_1\alpha}{\beta_1+\delta_2+\beta_2 y^V} + \delta_1\right)} & 0 \\ 0 & \sqrt{y^V\left(\frac{\beta_2\alpha x^V}{\beta_1+\delta_2+\beta_2 y^V} + \delta_1\right)} \end{pmatrix}\begin{pmatrix} dW_t^x \\ dW_t^y \end{pmatrix}.\end{aligned} \tag{12}$$

Inserting the deterministic coexistence equilibrium (Eq. (7)), we obtain

$$d\mathbf{U} = \underbrace{\begin{pmatrix} 0 & -\frac{\delta_1^2}{\alpha} \\ \alpha - \delta_1 - \frac{\delta_1\delta_2}{\beta_1} & \delta_1\left(\frac{\delta_1(\beta_1+\delta_2)}{\beta_1\alpha} - 1\right) \end{pmatrix}}_{=A}\mathbf{U}dt + \underbrace{\begin{pmatrix} \sqrt{\frac{2\beta_1\delta_1}{\beta_2}} & 0 \\ 0 & \sqrt{\frac{2\alpha\beta_1 - 2\delta_1(\beta_1+\delta_2)}{\beta_2}} \end{pmatrix}}_{=B}\begin{pmatrix} dW_t^x \\ dW_t^y \end{pmatrix}. \tag{13}$$

This stochastic process is a two-dimensional Ornstein-Uhlenbeck process. Its stationary covariance matrix Σ reads (Czuppon and Pfaffelhuber, 2018, Theorem 3)

$$\Sigma = \frac{(\widetilde{A} - \mathrm{tr}(\widetilde{A})I_2)BB^\top(\widetilde{A}^\top - \mathrm{tr}(\widetilde{A})I_2) + \det(\widetilde{A})BB^\top}{2\det(\widetilde{A})\mathrm{tr}(\widetilde{A})}, \tag{14}$$

where $\widetilde{A} = -A$ and I_2 is the two-dimensional identity matrix. Inserting the matrices as defined in Eq. (13) we find the rescaled stationary covariance matrix $\Sigma^* = \frac{\Sigma}{V}$

$$\Sigma^* = \frac{1}{V}\begin{pmatrix} \frac{\beta_1(2\alpha\beta_1 - \delta_1\delta_2)}{\beta_2(\alpha\beta_1 - \delta_1(\beta_1+\delta_2))} & \frac{\alpha\beta_1}{\beta_2\delta_1} \\ \frac{\alpha\beta_1}{\beta_2\delta_1} & \frac{\alpha\beta_1(\alpha+\delta_1)}{\beta_2\delta_1^2} \end{pmatrix}. \tag{15}$$

Writing $\xi = \alpha\beta_1/(\beta_2\delta_1)$ for the covariance term, we can rewrite this as

$$\Sigma^* = \frac{1}{V}\begin{pmatrix} x^*(1 + \frac{\xi}{y^*} + \frac{x^*}{y^*}) & \xi \\ \xi & \xi(1 + \frac{\xi}{x^*}) \end{pmatrix}. \tag{16}$$

Plugging everything into Eq. (13) and rearranging, we find that the stationary distribution of the two-dimensional TE numbers, which we denote by ψ^*, is given by

$$\psi^* \sim \mathcal{N}\left(\begin{pmatrix} x^* \\ y^* \end{pmatrix}, \Sigma^*\right). \tag{17}$$

The stationary variance of the autonomous TE, as indicated by the covariance matrix in Eq. (16), depends on its own mean, x^*, the mean of the nonautonomous TE, y^*, and the covariance of the

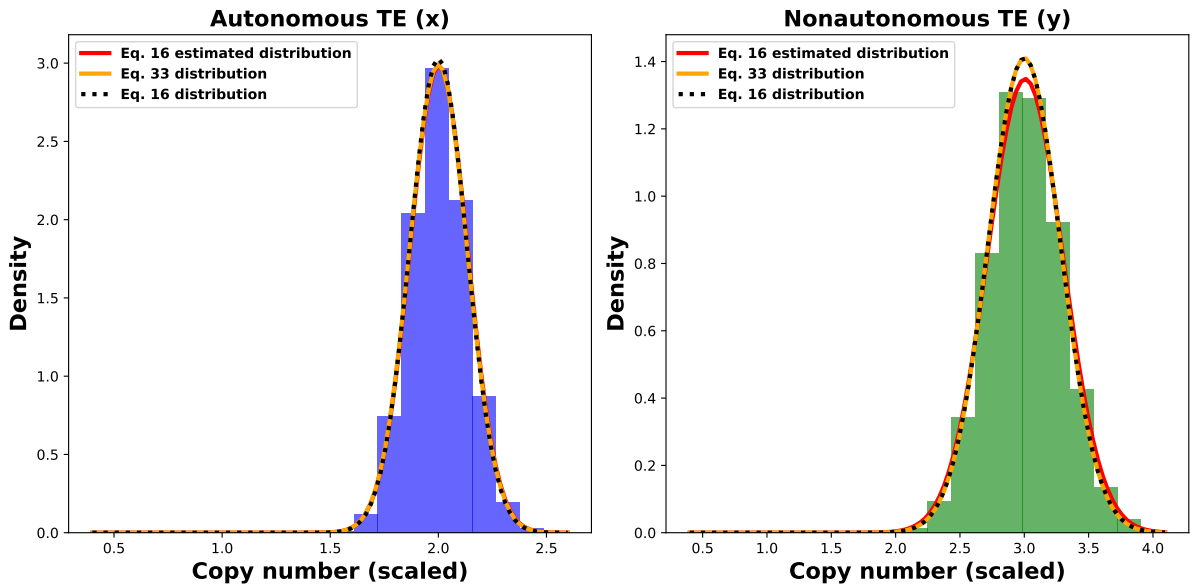

Figure 4: **Comparison of theoretical stationary distributions of TE numbers to stochastic simulations.** Autonomous (left) and nonautonomous (right) TE number histograms are obtained from 10,000 data points of a single stochastic simulation run for 1,000,000 time steps and sampled every 100 time steps (the equilibrium is already reached at that time, see Fig. 3). Parameter values are the standard parameter set (Table 1), resulting in theoretical mean TE numbers of $x^* = 2$ and $y^* = 3$ (Eq. (7)) and theoretical TE stationary variances of $\sigma^2_{x^*} = 0.017$, $\sigma^2_{y^*} = 0.08$ (Eq. 16) and $\sigma^2_{x^*} = 0.018$, $\sigma^2_{y^*} = 0.08$ (Eq. 33). The dashed, black line shows the linear noise approximation from the main text, and the stationary variance computed with the central limit theorem is shown by solid orange lines. Additionally, we plot the estimated stationary distribution (red, solid) computed with Eq. (16) and estimated x^*, y^* and γ values from the data. The estimates are $\hat{x}^* = 2$ and $\hat{y}^* = 3.01$ and an estimated covariance $\hat{\xi} = 0.017$. For comparison, the theoretical covariance is $\xi = 0.016$.

TEs in stationarity, ξ. The stationary variance of the nonautonomous TE, however, depends only on the covariance, ξ, and the mean value of the autonomous TE, x^*, but not on its own mean, y^*. Additionally, we note that it substantially depends on the covariance. The covariance itself, given by $\alpha\beta_1/\beta_2\delta_1 = \alpha x^*/\delta_1$, can be interpreted as the overall average number of complexes produced in stationarity. This implies that the stationary variance of nonautonomous TEs is strongly affected by the complex (or transposition machinery) encoded by the autonomous TE.

In Fig. 4 we compare our theoretical prediction of the stationary distribution to stochastic simulations and find a very good fit. We also plot the stationary distribution found through the central limit theorem (Eq. (33) in Appendix D) and see that for our parameters there is no visible difference between the two distributions. In fact, we find that the stationary variance of the nonautonomous TE and covariance are exactly the same. The stationary variance of the autonomous TE differs on the scale $O(1/V)$ (Eq. (34) in Appendix D). In Fig. 4, we also compute an empirical stationary distribution, where we estimate the equilibrium TE values, x^* and y^*, and the covariance ξ from the data and then use Eq. (17) to compute the stationary variances. The empirical stationary distribution fits the analytical prediction and data perfectly for the autonomous TE type, and differs slightly from the analytical distribution for the nonautonomous TE type.

Similar to the comparison of mean values of TEs in stationarity, we now provide analogous statements for the stationary variances. We denote the stationary variances of the autonomous and nonautonomous TEs as $\sigma^2_{x^*} = x^*(1 + \xi/y^* + x^*/y^*)$ and $\sigma^2_{y^*} = \xi(1 + \xi/x^*)$, respectively.

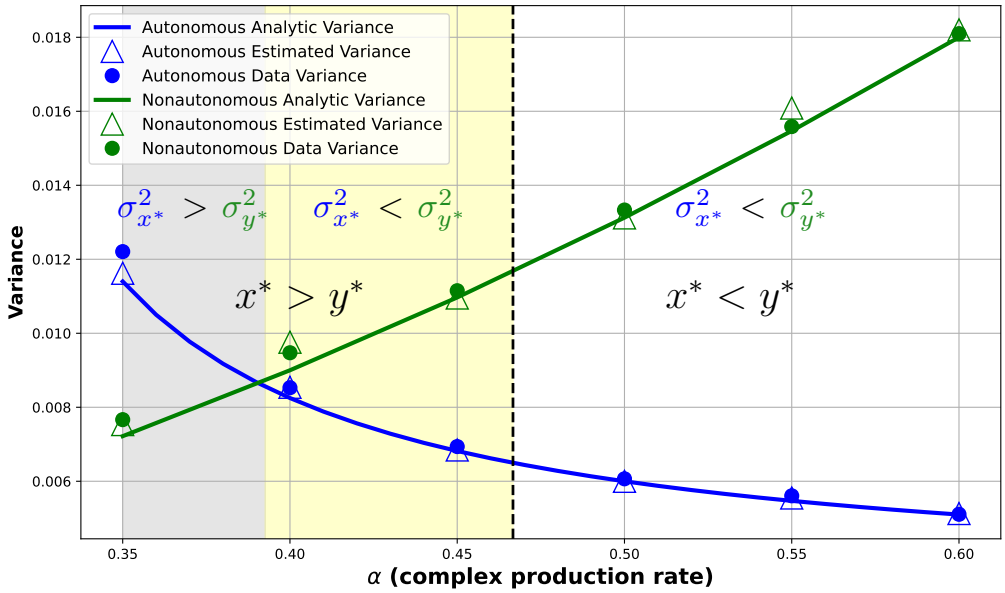

Figure 5: **Graphical representation of Proposition 2.** The figure shows the simulated (data), analytic and estimated variances of the autonomous and nonautonomous TEs interaction for constant parameter values $\beta_1 = 0.3$, $\beta_2 = 0.4$, $\delta_1 = 0.2$, $\delta_2 = 0.1$, and varying alpha values, as indicated. The figure shows that the relative copy numbers of the TEs depend on the rate of complex production by the autonomous TE, α. If the mean copy number of the autonomous TE is less than that of the nonautonomous TE (right of the dashed line), then the autonomous TE's stationary variance is less than that of the nonautonomous TE (white background). Conversely, if the mean copy number of the autonomous TE is greater than that of the nonautonomous TE (left of the dashed line), then the stationary variance of the autonomous TE can be greater (yellow), equal, or less (gray) than that of the nonautonomous TE, depending on the threshold value of $\gamma = 0.39$ for our parameter set.

Proposition 2. *Let the coexistence equilibrium (x^*, y^*) be locally stable. Then we have:*

(a) If $x^* \leq y^*$, then $\sigma^2_{x^*} < \sigma^2_{y^*}$.

(b) Set $\gamma = 1 + \frac{x^*}{y^*} - \frac{\alpha}{\alpha+\delta_1}$ and let $x^* > y^*$. We then have:

(i) If $\frac{\alpha}{\delta_1} > \gamma$, then $\sigma^2_{x^*} < \sigma^2_{y^*}$,

(ii) if $\frac{\alpha}{\delta_1} < \gamma$, then $\sigma^2_{x^*} > \sigma^2_{y^*}$,

(iii) if $\frac{\alpha}{\delta_1} = \gamma$, then $\sigma^2_{x^*} = \sigma^2_{y^*}$.

The proof is provided in Appendix B.

Proposition 2 shows the stationary variances of the two types of TEs and the relationship with their mean values. Importantly, we find that the stationary variance of the nonautonomous TE is always larger than that of the autonomous TE if the nonautonomous TE has a larger equilibrium value. The case where the mean copy number of the autonomous TE is larger than that of the nonautonomous TE is more involved, i.e., no simple prediction about the relationship of the stationary variances is possible. Fig. 5 visualizes these different scenarios as we vary the complex production rate α.

3.3 Effects of silencing on the TEs

Based on the results so far, we observed that nonautonomous TEs can be interpreted as having a regulatory effect on TE proliferation. To further elucidate this regulatory role, we now investigate the impact of potential host silencing on TE dynamics. We conducted simulations of the trap model described in the Model section to investigate if host silencing can be evaded under controlled TE dynamics as induced by an autonomous-nonautonomous TE pair. Fig. 6 shows the relationship between silencing rates and the impact of silencing on TE dynamics. Notably, we observe that there is minimal influence on expected TE dynamics at small silencing rates (5×10^{-6} to 9×10^{-6}). However, as silencing rates increase, a pronounced impact on TE dynamics emerges. We suspect that the final generation time of the simulation, 2000 in Fig. 6, does not affect the general pattern of a threshold silencing rate above which TE transposition is efficiently suppressed. The exact location of this silencing threshold, however, might change with final generation time. Overall, this pattern suggests that the limited impact of silencing on TEs at very low silencing rates can be attributed to the nonautonomous TE's regulation of excessive TE proliferation. We also observe that there is no substantial difference in the impact of host silencing on both types of TEs. That is, both TE types are equally distant (or close) to their respective stationary distributions as measured on the y axis in Fig. 6, meaning that silencing impacts both TE types equally strong.

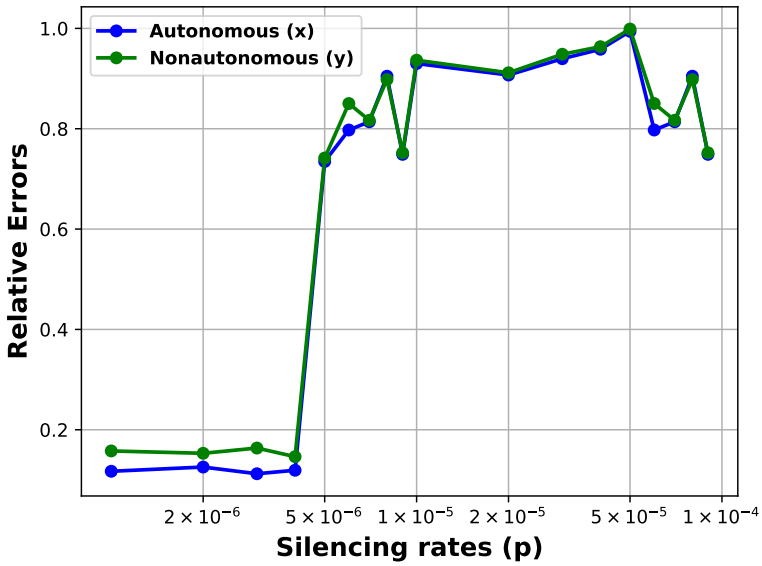

Figure 6: **Effect of silencing on TE dynamics.** The plot illustrates the relationship between silencing rates and the relative error of the variances in copy numbers of the autonomous and nonautonomous TEs. The relative error is defined as $\frac{|\sigma^2(p)-\sigma^2(0)|}{\sigma^2(0)}$. We simulated the trap model across various silencing rates, spanning from 10^{-6} to 9×10^{-5}, repeated 20 times to account for stochastic variability over 2000 generations in a population of 1000 individuals. Relative errors of TE copy numbers were computed for the averages of each rate compared to the absence of silencing. At low silencing rates (1×10^{-6} to 4×10^{-6}), silencing exerts minimal influence; however, as the silencing rate increases, a significant impact is observed, resulting in TE inactivation. Remaining parameters are their default values (Table 1).

4 Discussion

We studied a previously described model of the interaction of nonautonomous and autonomous transposable elements (Eq. (5); Xue and Goldenfeld (2016)). To analyze the system, we applied a time scale separation, where the numbers of TEs change on a slow time scale and the intermediate complex, necessary for TE transposition, is comparably short-lived (fast time scale). Based on this time scale separation, we first investigated the stability of the equilibria in the deterministic system and then quantified the stationary distribution of the stochastic model.

In the deterministic model, we find that stable coexistence of the two TEs is possible if the autonomous TE exhibits exponential growth in the absence of the nonautonomous TE (Eq. (10)). In other words, we find that nonautonomous TEs, in form of their transposition parameter β_2, do not directly contribute to the stability of the TE population (see also Appendix C for the more general model with different TE deactivation rates). Yet, it is their presence that keeps the system stable, which is mediated through their dependence on the transposition machinery of autonomous TEs for their mobility. This has prompted their labeling as "hyperparasitic", "superparasitic" or "parasites of parasites" (Startek et al., 2013; Robillard et al., 2016; Suh, 2019), considering that TEs propagate as parasites of the host. However, our analyses reveal that their role extends beyond mere hyperparasitism; an increase in their rate of transposition, β_2, results in a reduction of the autonomous TE equilibrium (Eq. (7)), indicating a regulatory role in controlling excessive TE proliferation (Rio, 1991; Hartl et al., 1992). This controlled maintenance may serve as a mechanism to prevent bursts of TE proliferation that could have deleterious effects on the host genome (Werren, 2011). Additionally, this low proliferation of TEs in a genome may less likely trigger host defenses, potentially leading to long-term persistence of the TE population (Hayward and Gilbert, 2022). Thus, TEs engage in a form of specialization: autonomous TEs encode the transposition machinery necessary for transposition, while nonautonomous TEs regulate TE proliferation, potentially enhancing the overall fitness of the TE community. This specialization supports the ecological perspective of the genome as an ecosystem (Venner et al., 2009; Linquist et al., 2015; Kremer et al., 2020). The autonomous-nonautonomous TE interaction would for example correspond to a cooperator-cheater analogy, wherein the cooperator, the autonomous TE, produces an essential public good necessary for reproduction (Moreno-Fenoll et al., 2017; Rosazza et al., 2023), here the transposition machinery, and the cheating type that does not produce the public good corresponds to nonautonomous TEs.

Previous population genetic models of autonomous-nonautonomous TE dynamics did not find stable coexistence (Brookfield, 1996; Le Rouzic and Capy, 2006; Startek et al., 2013). This contradicts empirical examples, for instance L1 and Alu elements in the human genome that seem to be active and coexisting since millions of years in the human genome lineage (Kazazian, 2004). One important difference from our model to previous models is that we account explicitly for the molecular mechanisms of transposition. While this might already explain the difference to previous results, it is also possible that previous models failed to explain coexistence because in these models autonomous TEs give rise to nonautonomous TEs through mutation. Relaxing this condition indeed produced relatively stable cyclic dynamics of autonomous and nonautonomous TEs in simulations (Le Rouzic and Capy, 2006). Our assumption of 'unrelated' autonomous and nonautonomous TE families is in line with empirical observations, e.g. L1 and Alu elements in the human genome and also the RLG_*Wilma* and RLG_*Sabrina* elements in the wheat genome seem to be unrelated (Kazazian, 2004; Wicker et al., 2021). Another difference to previous models is that we did not model any fitness effects of the TEs on the host. The consequences of this assumption remain to be studied, though we do not suspect that adding deleterious fitness effects of TEs on the host will change the qualitative behavior of our model.

However, it is important to emphasize that not all autonomous-nonautonomous TE interactions will result in long-term coexistence. For example, the empirical study by Robillard et al. (2016) demonstrated autonomous-nonautonomous TE dynamics that did not result in long-term coexis-

tence. They studied the autonomous *Mos1* and nonautonomous *peach* elements of the *mariner* family in *Drosophila Melanogaster*. Their findings revealed that when both TEs are present in the same genome, the nonautonomous TEs amplify significantly, indicative of a very large value nonautonomous transposition rate β_2 compared to the autonomous transposition rate β_1, which adversely affects the survival and reproductive activity of the autonomous TE. This empirical observation fits with our model prediction because for transposition rates $\beta_2 \gg \beta_1$, the autonomous equilibrium $x^* = \beta_1/\beta_2$ converges to zero.

Our main result is the computation of the stationary variance in the stochastic model (Eq. (17)). The stationary distribution, which we derive from a linear noise approximation, is a normal distribution centered around the deterministic equilibrium (Eq. (7)); derivation of the stationary distribution with the more exact central limit theorem gives almost exactly the same result (Eq. (33) in Appendix D). Surprisingly, the covariance matrix in stationarity takes a very specific form in our analysis in the main text (Eq. (16)). We find that the stationary variances of the autonomous and nonautonomous TEs can be rewritten in terms of the covariance between the two TEs and the deterministic equilibria. Importantly, this opens the possibility to test this TE model against data. Given multiple sequences from the same species and a known autonomous-nonautonomous TE pair, e.g. active L1 and Alu copy numbers obtained from different human genome sequences (Hancks and Kazazian, 2012; Dewannieux et al., 2003), one could compare the observed variance of the elements to the predicted form, which is computed from the sample means and the sample covariance.

Additionally, the stationary covariance matrix provides further support to the regulatory role of nonautonomous TEs. Each entry in the matrix scales inversely with the nonautonomous transposition rate β_2. That is, stochastic fluctuations in TE copy numbers are small if β_2 is large. Thus, nonautonomous TEs not only affect the equilibrium value of autonomous TEs but regulate the overall variability of the TE dynamics.

To investigate if this active, host-unregulated TE transposition is indeed possible over long periods of time, we have extended our model to account for host regulation. Due to the threats TEs pose to genome stability, hosts have evolved multiple mechanisms to mitigate the harmful effects of TEs (Bhat et al., 2022). One such mechanism involves Piwi-interacting RNA (piRNA), which associates with Piwi proteins to regulate TE transposition in germline cells (Slotkin and Martienssen, 2007). In this regulation mechanism, once a TE transposes into a piRNA cluster, all TE copies in the genome are silenced preventing any further TE activity (Fig. 2). This model has recently been termed *trap model* (Kofler, 2019, 2020; Tomar et al., 2023). Incorporating the trap model into the model of autonomous-nonautonomous TE interaction, we find that long-term proliferation of TEs and evasion of host regulation is indeed possible, at least if the silencing rate is low enough. A similar qualitative result has been described in a simulation study, where the abundance of piRNA clusters, which is assumed to be proportional to the silencing rate, has to exceed 0.2% of the genome to efficiently suppress TE transposition (Kofler, 2020). This rate is much higher than our silencing threshold, though our model does not account for recombination and deleterious fitness effects of TEs, which prevents quantitative comparison between the two models. The interaction of autonomous and nonautonomous TEs can therefore be interpreted as a TE (self-)regulation mechanism to preclude host regulation and ensure long-term transposition activity.

We further explored the relationship between the two types of TEs. We found that the relationship of copy numbers of the two TEs are influenced by the interplay between the average number of complexes (transposition machinery) encoded by the autonomous TE and its transposition rate β_1, as presented in Proposition 1. This interaction explains the mechanisms underlying the varying copy numbers of TEs (Schulman and Wicker, 2013). We discovered that if the transposition rate of the autonomous TE β_1 is low, the average number of complexes required for the nonautonomous TE to be more abundant than the autonomous TE increases. Conversely, if the transposition rate of the autonomous TE is high, the average number of complexes required for the nonautonomous TE

to be more abundant is low. These insights help explain why nonautonomous TEs are often more abundant than autonomous TEs (Robillard et al., 2016). Examples include the Alu element, which accounts for approximately 1.1 million copies with about 852 active ones, and the L1 element, which accounts for approximately $516\ 000$ copies with about $40 - 50$ active ones in the human genome (Hancks and Kazazian, 2012).

We also examined the relative variation of TE copy number to their mean copy number as presented in Proposition 2. Our observations indicate that when the mean copy number of autonomous TEs is lower than that of nonautonomous TEs, the variance of autonomous TEs is smaller than that of nonautonomous TEs. Conversely, if the mean copy number of autonomous TEs exceeds that of nonautonomous TEs, no simple prediction of the relationship between stationary variances of the TEs is possible. Variations in TE copy number can also shed light on genome stability, with higher variance indicating greater genomic instability, while lower variance, regulated by nonautonomous TEs or the host, may signify genomic regions with more stable TE content and reduced activity rates (Bhat et al., 2022).

In conclusion, we analyzed a stochastic model of autonomous-nonautonomous TE interactions. This interaction can produce a stable coexistence of both TE types and therefore is a potential mechanism to explain the maintenance of TE transposition in genome lineages over long periods of time. Additionally, our theoretically predicted stationary distribution of TE copy numbers is suited to be compared to empirical data of (active) TE copy numbers because its special form does not require knowledge about TE transposition or deactivation rates.

Acknowledgements

AO has received funding from the project FlyInnovation (CZ 294/1-1) within the GEvol priority program (SPP 2349) funded by the German Science Foundation (DFG). We are grateful to the High Performance Computing service of the University of Münster for providing computational resources on the computer cluster PALMA II.

Appendix

A Proof of Proposition 1

Proof. Statements (b) and (c) follow directly from statement (a). To prove statement (a), we have

$$\begin{aligned} x^* < y^* &\iff \frac{\beta_1}{\beta_2} < \frac{\beta_1\alpha - \delta_1\delta_2 - \beta_1\delta_1}{\beta_2\delta_1}, \\ &\iff \beta_1\delta_1 < \beta_1\alpha - \delta_1\delta_2 - \beta_1\delta_1, \\ &\iff 2\beta_1\delta_1 + \delta_1\delta_2 < \beta_1\alpha, \\ &\iff 2 + \frac{\delta_1\delta_2}{\beta_1\delta_1} < \frac{\beta_1\alpha}{\beta_1\delta_1}, \\ &\iff \frac{\alpha}{\delta_1} > \frac{\delta_2}{\beta_1} + 2. \end{aligned}$$

This concludes the proof. □

Visualization of Proposition 1. In Fig. 7 we show how the average number of complexes produced by an autonomous TE (x-axis) affects the relationship between mean copy numbers of autonomous and nonautonomous TEs.

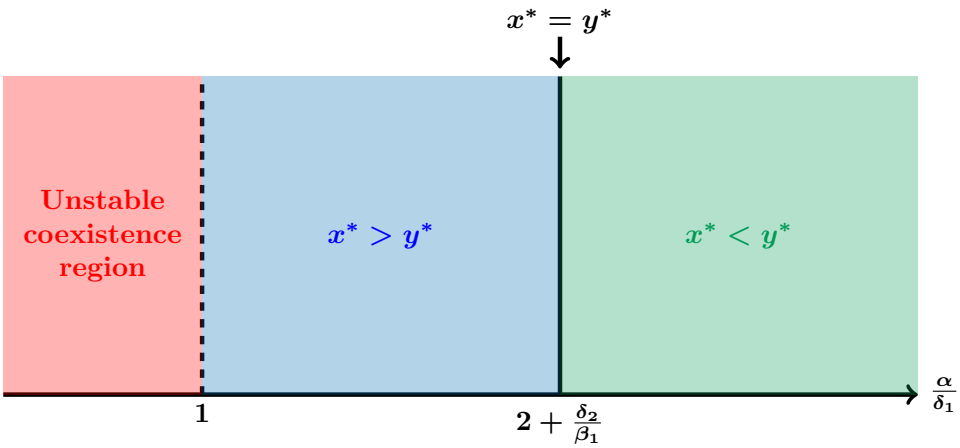

Figure 7: **Relative copy numbers of the autonomous-nonautonomous TE interaction.** The average number of complexes produced by an autonomous TE, α/δ_1, needs to exceed 1 for stable coexistence to occur (dashed line). If it exceeds the value $2+\delta_2/\beta_1$, then nonautonomous TEs are more abundant compared to autonomous TEs (green background), if it is between 1 and $2+\delta_2/\beta_1$, then autonomous TEs are more abundant (blue background).

B Proof of Proposition 2

Proof. To prove Proposition 2, we first determine the threshold value x^*/y^* when $\sigma^2_{x^*}$ is equal to $\sigma^2_{y^*}$. To this end, we simplify

$$\begin{aligned}
& \sigma^2_{x^*} = x^*\left[1+\frac{x^*}{y^*}\left(1+\frac{\alpha}{\delta_1}\right)\right] = x^*\frac{\alpha}{\delta_1}\left(1+\frac{\alpha}{\delta_1}\right) = \sigma^2_{y^*} \\
\iff \quad & \frac{\delta_1}{\alpha+\delta_1}+\frac{x^*}{y^*} = \frac{\alpha}{\delta_1} \\
\iff \quad & \frac{\alpha-\alpha+\delta_1}{\alpha+\delta_1}+\frac{x^*}{y^*} = \frac{\alpha}{\delta_1} \\
\iff \quad & 1-\frac{\alpha}{\alpha+\delta_1}+\frac{x^*}{y^*} = \frac{\alpha}{\delta_1} \\
\iff \quad & \frac{x^*}{y^*} = \frac{\alpha}{\delta_1}+\frac{\alpha}{\alpha+\delta_1}-1.
\end{aligned} \tag{18}$$

(a) In this case, we have $x^* \leq y^*$. With Proposition 1 (a) and (c), we then also have $\frac{\alpha}{\delta_1} \geq 2+\frac{\delta_2}{\beta_1}$. Now, comparing this to Eq. (18), we see that the left hand side is smaller than 1, and the right hand side is larger than 1, so that we find:

$$\underbrace{\frac{x^*}{y^*}}_{\leq 1} < \underbrace{\frac{\alpha}{\delta_1}+\frac{\alpha}{\alpha+\delta_1}-1}_{\geq 1+\frac{\delta_2}{\beta_1}+\frac{\alpha}{\alpha+\delta_1}>1}. \tag{19}$$

This implies that $\sigma^2_{x^*} < \sigma^2_{y^*}$.

(b) Here, we have $x^* > y^*$. Writing $\gamma = 1-\frac{\alpha}{\alpha+\delta_1}+\frac{x^*}{y^*}$, we and plugging this into the second

last line in Eq. (18), we then directly have that:

$$\text{(i)} \qquad \text{if } \gamma < \frac{\alpha}{\delta_1}, \quad \text{then } \sigma^2_{x^*} < \sigma^2_{y^*}, \tag{20}$$

$$\text{(ii)} \qquad \text{if } \gamma > \frac{\alpha}{\delta_1}, \quad \text{then } \sigma^2_{x^*} > \sigma^2_{y^*}, \tag{21}$$

$$\text{(iii)} \qquad \text{if } \gamma = \frac{\alpha}{\delta_1}, \quad \text{then } \sigma^2_{x^*} = \sigma^2_{y^*}. \tag{22}$$

□

C Model with different TE deactivation rates

In the main text we have assumed that both TEs are deactivated at the same (scaled) rate δ_1. Here, we study the more general model where we allow for different deactivation rated δ_x and δ_y. The model in the main text is recovered by setting $\delta_x = \delta_y = \delta_1$.

We first note that the equilibrium complex copy number C^* is unaffected and remains as given in Eq. (3). The stochastic differential equations are then given by

$$\begin{aligned} dx^V &= (\beta_1 C^* - \delta_x x^V)dt + \sqrt{\frac{\beta_1 C^* + \delta_x x^V}{V}} dW_t^x, \\ dy^V &= (\beta_2 C^* y^V - \delta_y y^V)dt + \sqrt{\frac{\beta_1 C^* y^V + \delta_y y^V}{V}} dW_t^y, \end{aligned} \tag{23}$$

The non-trivial deterministic equilibrium of this model reads

$$(x^*, y^*) = \left(\frac{\beta_1 \delta_y}{\beta_2 \delta_x}, \frac{\alpha\beta_1 - \delta_x\delta_2 - \delta_x\beta_1}{\beta_2\delta_x} \right). \tag{24}$$

This equilibrium exists if $\alpha\beta_1 - \delta_x\delta_2 - \delta_x\beta_1 > 0$, which is the same condition as in Eq. (8) in the main text. Moreover, the equilibrium is locally stable if it exists (determinant-trace condition evaluated in the supplemental *Mathematica* notebook). We can therefore conclude that the TE-specific deactivation rate does not affect the local stability of the system and that the biological interpretations drawn in the main text extend to this more general case.

To derive the stationary distribution, we repeat the same steps as in the main text to find the following stationary covariance matrix:

$$\Sigma = \begin{pmatrix} \frac{\beta_1(\alpha\beta_1(\delta_x+\delta_y)-\delta_2\delta_x\delta_y)}{\beta_2\delta_x(\alpha\beta_1-\delta_x(\beta_1+\delta_2))} & \frac{\alpha\beta_1}{\beta_2\delta_x} \\ \frac{\alpha\beta_1}{\beta_2\delta_x} & \frac{\alpha\beta_1(\alpha+\delta_y)}{\beta_2\delta_x\delta_y} \end{pmatrix}, \tag{25}$$

which reduces to Eq. (15) for $\delta_x = \delta_y = \delta_1$. Again, rewriting the covariance as $\xi = \alpha\beta_1/(\beta_2\delta_x)$, we can rewrite the stationary variance of y as $\sigma^2_{y^*} = \xi(1 + \xi/x^*)$. However, we were not able to find a simplification of the stationary variance of x as in the main text. We arrive at

$$\sigma^2_{x^*} = x^* \left(1 + \frac{\delta_x}{\delta_y} \frac{1}{y^*} (x^* + \xi) \right). \tag{26}$$

D Approximating the stationary distribution with the method from Kang et al. (2014)

Here, we provide a second way to approximate the stationary distribution. Instead of using the equilibrium value C^* whenever possible, which we did in the main text, we now account for the

stochastic nature of the intermediary complex. Under a time scale separation, as we apply it, this method was introduced as a central limit theorem by Kang et al. (2014). We will follow the application of this method as presented in Appendix A of Czuppon and Pfaffelhuber (2018). To this end, we first write down the infinitesimal generator L^V (applied to a auxiliary function $f(C, x^V, y^V)$) of the rescaled model as stated in Eq. (2):

$$\begin{aligned}
L^V f(C,x,y) &= V\alpha x^V (f(C+1,x,y) - f(C,x,y)) \\
&\quad + V\beta_1 C(f(C-1,x+1/V,y) - f(C,x,y)) \\
&\quad + V\beta_2 Cy(f(C-1,x,y+1/V) - f(C,x,y)) \\
&\quad + V\delta_1 x(f(C,x-1/V,y) - f(C,x,y)) \\
&\quad + V\delta_1 y(f(C,x,y-1/V) - f(C,x,y)) \\
&\quad + V\delta_2 C(f(C-1,x,y) - f(C,x,y)) \\
&\approx (\beta_1 C - \delta_1 x)\partial_x f(C,x,y) + (\beta_2 Cy - \delta_1 y)\partial_y f(C,x,y) \\
&\quad V\alpha x(f(C+1,x,y) - f(C,x,y)) \\
&\quad + V(\beta_1 C + \beta_2 Cy + \delta_2 C)(f(C-1,x,y) - f(C,x,y)) \\
&= L_1^V f(C,x,y) + V\ L_2^V f(C,x,y)\,,
\end{aligned} \tag{27}$$

where L_1^V is the infinitesimal generator of the 'slow' subsystem and L_2^V corresponds to the 'fast' subsystem. The deterministic dynamics under the time scale separation are given by

$$\begin{pmatrix} \frac{dx^V}{dt} \\ \frac{dy^V}{dt} \end{pmatrix} = \begin{pmatrix} \beta_1 C - \delta_1 x^V \\ \beta_2 C y^V - \delta_2 y^V \end{pmatrix} = F(C, x^V, y^V)\,. \tag{28}$$

Following step ❷ in Appendix A from Czuppon and Pfaffelhuber (2018), the idea is to find a function $h(C,x,y)$ so that $L_2^V h^V \approx F(C,x,y) - F(C^*,x,y)$. Setting $h^V(C,x,y) = (-C\beta_1/(\beta_1+\beta_2 y+\delta_2), -C\beta_2 y/(\beta_1+\beta_2 y+\delta_2)$, we find

$$\begin{aligned}
L_2^V h^V(C,x,y) &= \begin{pmatrix} \alpha x \frac{\beta_1(-(C+1)+C)}{\beta_1+\beta_2 y+\delta_2} + C(\beta_1+\beta_2 y+\delta_2)\frac{\beta_1(-(C-1)+C)}{\beta_1+\beta_2 y+\delta_2} \\ \alpha x \frac{\beta_2 y(-(C+1)+C)}{\beta_1+\beta_2 y+\delta_2} + C(\beta_1+\beta_2 y+\delta_2)\frac{\beta_2 y(-(C-1)+C)}{\beta_1+\beta_2 y+\delta_2} \end{pmatrix} \\
&= \begin{pmatrix} \beta_1\left(C - \frac{\alpha x}{\beta_1+\beta_2 y+\delta_2}\right) \\ \beta_2 y\left(C - \frac{\alpha x}{\beta_1+\beta_2 y+\delta_2}\right) \end{pmatrix} \\
&= \begin{pmatrix} \beta_1(C-C^*) \\ \beta_2 y(C-C^*) \end{pmatrix}.
\end{aligned} \tag{29}$$

Lastly, we have to compute the quadratic variation (❹ in Czuppon and Pfaffelhuber (2018)). We now denote by $\zeta_k = (\zeta_k^C, \zeta_k^x, \zeta_k^y)$ the change in numbers due to the kth transition in Eq. (1) and by λ_k the corresponding transition rate. Then, we find that with $z^{\otimes 2} = zz^\top$ and $\mathcal{K}$ the number of

transitions, the quadratic variation is given by

$$
\begin{aligned}
&\frac{1}{V}\sum_{k\in\mathcal{K}}\int_0^t \Big((\zeta_k^x,\zeta_k^y)^\top + h^V(C(s-),x(s-),y(s-)\\
&\qquad -h^V\left(C(s-)+\zeta_k^C, x(s-)+\frac{\zeta_k^x}{V}, y(s-)+\frac{\zeta_k^y}{V}\right)\Big)^{\otimes 2}\lambda_k(C(s),x(s),y(s))ds\\
&\approx \int_0^t \alpha x\begin{pmatrix}\frac{\beta_1}{\beta_1+\beta_2 y+\delta_2}\\ \frac{\beta_2 y}{\beta_1+\beta_2 y+\delta_2}\end{pmatrix}^{\otimes 2} + \beta_1 C\begin{pmatrix}1-\frac{\beta_1}{\beta_1+\beta_2 y+\delta_2}\\ -\frac{\beta_2 y}{\beta_1+\beta_2 y+\delta_2}\end{pmatrix}^{\otimes 2} + \beta_2 C y\begin{pmatrix}-\frac{\beta_1}{\beta_1+\beta_2 y+\delta_2}\\ 1-\frac{\beta_2 y}{\beta_1+\beta_2 y+\delta_2}\end{pmatrix}^{\otimes 2}\\
&\qquad + \delta_1 x\begin{pmatrix}-1\\ 0\end{pmatrix}^{\otimes 2} + \delta_1 y\begin{pmatrix}0\\ -1\end{pmatrix}^{\otimes 2} + \delta_2 C\begin{pmatrix}-\frac{\beta_1}{\beta_1+\beta_2 y+\delta_2}\\ -\frac{\beta_2 y}{\beta_1+\beta_2 y+\delta_2}\end{pmatrix}^{\otimes 2} ds\\
&= \int_0^t \begin{pmatrix}\frac{(\alpha x\beta_1^2+\beta_1 C(\delta_2+\beta_2 y)^2+\beta_2 C y\beta_1^2+\delta_2 C\beta_1^2)}{(\beta_1+\beta_2 y+\delta_2)^2}+\delta_1 x & \frac{(\alpha x\beta_1\beta_2 y-\beta_1\beta_2 C y(\beta_2 y+3\delta_2+\beta_1))}{(\beta_1+\beta_2 y+\delta_2)^2}\\ \frac{(\alpha x\beta_1\beta_2 y-\beta_1\beta_2 C y(\beta_2 y+3\delta_2+\beta_1))}{(\beta_1+\beta_2 y+\delta_2)^2} & \frac{(\alpha x\beta_2^2 y^2+\beta_1 C\beta_2^2 y^2+\beta_2 C y(\beta_1+\delta_2)^2+\delta_2 C\beta_2^2 y^2)}{(\beta_1+\beta_2 y+\delta_2)^2}+\delta_1 y\end{pmatrix} ds\,.
\end{aligned}
\tag{30}
$$

Evaluated in the equilibrium (C^*, x^*, y^*), we obtain for the quadratic variation

$$
\widetilde{B} = \begin{pmatrix}\frac{2\beta_1\delta_1}{\beta_2} & \frac{2\delta_1^2\delta_2(-\alpha\beta_1+\delta_1(\beta_1+\delta_2))}{\alpha^2\beta_1\beta_2}\\ \frac{2\delta_1^2\delta_2(-\alpha\beta_1+\delta_1(\beta_1+\delta_2))}{\alpha^2\beta_1\beta_2} & \frac{2\alpha\beta_1-2\delta_1(\beta_1+\delta_2)}{\beta_2}\end{pmatrix}. \tag{31}
$$

Now following the same steps as in the main text (Eqs. (13) and (14)) with $\widetilde{B}$ as just defined, we find

$$
\widetilde{\Sigma}^* = \frac{1}{V}\begin{pmatrix}\frac{\beta_1}{\beta_2}+\frac{2\delta_1^2\delta_2}{\alpha^2\beta_2}+\frac{\beta_1^2(\alpha+\delta_1)}{\beta_2(\alpha\beta_1-\delta_1(\beta_1+\delta_2))} & \frac{\alpha\beta_1}{\beta_2\delta_1}\\ \frac{\alpha\beta_1}{\beta_2\delta_1} & \frac{\alpha\beta_1(\alpha+\delta_1)}{\beta_2\delta_1^2}\end{pmatrix}. \tag{32}
$$

Compared to Eq. (15) only the variance term of the autonomous TE (top left entry) has changed. Again, writing $\xi = \alpha\beta_1/(\beta_2\delta_1)$, we can rewrite the stationary covariance matrix as

$$
\widetilde{\Sigma}^* = \frac{1}{V}\begin{pmatrix}x^*\left(1+2\frac{x^*}{\xi^2}\frac{\delta_2}{\beta_2}+\frac{x^*}{y^*}+\frac{\xi}{y^*}\right) & \xi\\ \xi & \xi\left(1+\frac{\xi}{x^*}\right)\end{pmatrix} = \begin{pmatrix}\widetilde{\sigma}_{x^*}^2 & \xi\\ \xi & \widetilde{\sigma}_{y^*}^2\end{pmatrix}. \tag{33}
$$

Contrarily to the less accurate method from the main text, we cannot rewrite the stationary variance of the autonomous TE, $\widetilde{\sigma}_{x^*}^2$, in terms of the steady states and the covariance. Instead, we need knowledge about two parameter ratios, δ_2/β_2 and α/δ_1, if we wanted to compare this stationary variance to data. The difference to the calculated variance in the main text, $\sigma_{x^*}^2$ is

$$
\frac{1}{V}\left(\widetilde{\sigma}_{x^*}^2 - \sigma_{x^*}^2\right) = \frac{2}{V}\frac{(x^*)^2}{\xi^2}\frac{\delta_2}{\beta_2} = \frac{2}{V}\frac{\delta_1^2\delta_2}{\alpha^2\beta_2}, \tag{34}
$$

which in our default parameter set amounts to 7.5×10^{-4}. This term becomes negligible if the rate of TE deactivation, δ_1, is very low, the rate of complex degradation, δ_2, is very low, the rate of complex production, α, is very high, or if the rate of nonautonomous TE transposition, β_2, is very high.

References

Anderson, D. F. and Kurtz, T. G. *Continuous Time Markov Chain Models for Chemical Reaction Networks*, page 342. Springer New York, 2011. doi: 10.1007/978-1-4419-6766-4_1.

Ball, K., Kurtz, T. G., Popovic, L., and Rempala, G. Asymptotic analysis of multiscale approximations to reaction networks. *The Annals of Applied Probability*, 16(4), 2006. doi: 10.1214/105051606000000420.

Bennett, P. M. Plasmid encoded antibiotic resistance: acquisition and transfer of antibiotic resistance genes in bacteria. *British Journal of Pharmacology*, 153, 2008. doi: 10.1038/sj.bjp.0707607.

Bennetzen, J. L. and Wang, H. The contributions of transposable elements to the structure, function, and evolution of plant genomes. *Annual Review of Plant Biology*, 65(1):505–530, 2014. doi: 10.1146/annurev-arplant-050213-035811.

Bhat, A., Ghatage, T., Bhan, S., Lahane, G. P., Dhar, A., Kumar, R., Pandita, R. K., Bhat, K. M., Ramos, K. S., and Pandita, T. K. Role of transposable elements in genome stability: Implications for health and disease. *International Journal of Molecular Sciences*, 23(14):7802, 2022. doi: 10.3390/ijms23147802.

Boeke, J. D. LINEs and *Alus* – the polyA connection. *Nature Genetics*, 16(1):6–7, 1997. doi: 10.1038/ng0597-6.

Brennecke, J., Aravin, A. A., Stark, A., Dus, M., Kellis, M., Sachidanandam, R., and Hannon, G. J. Discrete small RNA-generating loci as master regulators of transposon activity in *Drosophila*. *Cell*, 128(6):1089–1103, 2007. doi: 10.1016/j.cell.2007.01.043.

Brookfield, J. F. Y. Models of the spread of non-autonomous selfish transposable elements when transposition and fitness are coupled. *Genetical Research*, 67(3):199–209, 1996. doi: 10.1017/s0016672300033681.

Brookfield, J. F. and Badge, R. M. Population genetics models of transposable elements. *Genetica*, 100(1/3):281–294, 1997. doi: 10.1023/a:1018310418744.

Charlesworth, B. and Langley, C. H. The evolution of self-regulated transposition of transposable elements. *Genetics*, 112(2):359383, 1986. doi: 10.1093/genetics/112.2.359.

Charlesworth, B. Transposable elements in natural populations with a mixture of selected and neutral insertion sites. *Genetical Research*, 57(2):127134, 1991. doi: 10.1017/s0016672300029190.

Charlesworth, B. and Charlesworth, D. The population dynamics of transposable elements. *Genetical Research*, 42(1):1–27, 1983. doi: 10.1017/s0016672300021455.

Cooke, S. L., Shlien, A., Marshall, J., Pipinikas, C. P., Martincorena, I., Tubio, J. M., Li, Y., Menzies, A., Mudie, L., Ramakrishna, M., et al. Processed pseudogenes acquired somatically during cancer development. *Nature Communications*, 5(1), 2014. doi: 10.1038/ncomms4644.

Cosby, R. L., Chang, N.-C., and Feschotte, C. Host-transposon interactions: conflict, cooperation, and cooption. *Genes & Development*, 33(1718):1098–1116, 2019. doi: 10.1101/gad.327312.119.

Czech, B. and Hannon, G. J. One loop to rule them all: The ping-pong cycle and piRNA-guided silencing. *Trends in Biochemical Sciences*, 41(4):324–337, 2016. doi: 10.1016/j.tibs.2015.12.008.

Czuppon, P. and Pfaffelhuber, P. Limits of noise for autoregulated gene expression. *Journal of Mathematical Biology*, 77(4):1153–1191, 2018. doi: 10.1007/s00285-018-1248-4.

Czuppon, P. and Traulsen, A. Understanding evolutionary and ecological dynamics using a continuum limit. *Ecology and Evolution*, 11(11):5857–5873, 2021. doi: 10.1002/ece3.7205.

Dewannieux, M., Esnault, C., and Heidmann, T. LINE-mediated retrotransposition of marked Alu sequences. *Nature Genetics*, 35(1):41–48, 2003. doi: 10.1038/ng1223.

Doolittle, W. F. and Sapienza, C. Selfish genes, the phenotype paradigm and genome evolution. *Nature*, 284(5757):601–603, 1980. doi: 10.1038/284601a0.

Ethier, S. N. and Kurtz, T. G. *Markov Processes: Characterization and Convergence*. Wiley, 1986. doi: 10.1002/9780470316658.

Feschotte, C., Swamy, L., and Wessler, S. R. Genome-wide analysis of *mariner*-like transposable elements in rice reveals complex relationships with *Stowaway* Miniature Inverted Repeat Transposable Elements (MITEs). *Genetics*, 163(2):747–758, 2003. doi: 10.1093/genetics/163.2.747.

Gillespie, D. T. A general method for numerically simulating the stochastic time evolution of coupled chemical reactions. *Journal of Computational Physics*, 22(4):403–434, 1976. doi: 10.1016/0021-9991(76)90041-3.

Gillespie, D. T. Approximate accelerated stochastic simulation of chemically reacting systems. *The Journal of Chemical Physics*, 115(4):1716–1733, 2001. doi: 10.1063/1.1378322.

Hancks, D. C. and Kazazian, H. H. Active human retrotransposons: variation and disease. *Current Opinion in Genetics and Development*, 22(3):191–203, 2012. doi: 10.1016/j.gde.2012.02.006.

Hartl, D. L., Lozovskaya, E. R., and Lawrence, J. G. Nonautonomous transposable elements in prokaryotes and eukaryotes. *Genetica*, 86(13):47–53, 1992. doi: 10.1007/bf00133710.

Hayward, A. and Gilbert, C. Transposable elements. *Current Biology*, 32(17):R904–R909, 2022.

Kang, H.-W., Kurtz, T. G., and Popovic, L. Central limit theorems and diffusion approximations for multiscale Markov chain models. *The Annals of Applied Probability*, 24(2), 2014. doi: 10.1214/13-aap934.

Kazazian, H. H. Mobile elements: Drivers of genome evolution. *Science*, 303(5664):1626–1632, 2004. doi: 10.1126/science.1089670.

Kofler, R. Dynamics of transposable element invasions with piRNA clusters. *Molecular Biology and Evolution*, 36(7):1457–1472, 2019. doi: 10.1093/molbev/msz079.

Kofler, R. piRNA clusters need a minimum size to control transposable element invasions. *Genome Biology and Evolution*, 12(5):736–749, 2020. doi: 10.1093/gbe/evaa064.

Kremer, S. C., Linquist, S., Saylor, B., Elliott, T. A., Gregory, T. R., and Cottenie, K. Transposable element persistence via potential genome-level ecosystem engineering. *BMC Genomics*, 21(1), 2020. doi: 10.1186/s12864-020-6763-1.

Le Rouzic, A. and Capy, P. Population genetics models of competition between transposable element subfamilies. *Genetics*, 174(2):785–793, 2006. doi: 10.1534/genetics.105.052241.

Le Rouzic, A., Boutin, T. S., and Capy, P. Long-term evolution of transposable elements. *Proceedings of the National Academy of Sciences*, 104(49):19375–19380, 2007. doi: 10.1073/pnas.0705238104.

Linquist, S., Cottenie, K., Elliott, T. A., Saylor, B., Kremer, S. C., and Gregory, T. R. Applying ecological models to communities of genetic elements: the case of neutral theory. *Molecular Ecology*, 24(13):32323242, 2015. doi: 10.1111/mec.13219.

McClintock, B. Controlling elements and the gene. *Cold Spring Harbor Symposia on Quantitative Biology*, 21:197–216, 1956. doi: 10.1101/sqb.1956.021.01.017.

Montgomery, E. A., Huang, S. M., Langley, C. H., and Judd, B. H. Chromosome rearrangement by ectopic recombination in *Drosophila melanogaster*: Genome structure and evolution. *Genetics*, 129(4):1085–1098, 1991. doi: 10.1093/genetics/129.4.1085.

Moreno-Fenoll, C., Cavaliere, M., Martnez-Garca, E., and Poyatos, J. F. Eco-evolutionary feedbacks can rescue cooperation in microbial populations. *Scientific Reports*, 7(1), 2017. doi: 10.1038/srep42561.

Orgel, L. E. and Crick, F. H. C. Selfish DNA: the ultimate parasite. *Nature*, 284(5757):604–607, 1980. doi: 10.1038/284604a0.

Otto, S. P. and Day, T. *A Biologist's Guide to Mathematical Modeling in Ecology and Evolution*. Princeton Univ. Press, Princeton, NJ, 2007.

Rio, D. C. Regulation of *Drosophila* P element transposition. *Trends in Genetics*, 7(9):282–287, 1991. doi: 10.1016/0168-9525(91)90309-e.

Robillard, E., Le Rouzic, A., Zhang, Z., Capy, P., and Hua-Van, A. Experimental evolution reveals hyperparasitic interactions among transposable elements. *Proceedings of the National Academy of Sciences*, 113(51):14763–14768, 2016. doi: 10.1073/pnas.1524143113.

Rosazza, T., Eigentler, L., Earl, C., Davidson, F., and Stanley-Wall, N. Extracellular proteases are an essential public good supporting *Bacillus subtilis* growth through exogenous protein degradation. 2023. doi: 10.1101/2023.02.08.527645.

Schulman, A. H. and Wicker, T. A field guide to transposable elements. *Plant Transposons and Genome Dynamics in Evolution*, pages 15–40, 2013. doi: 10.1002/9781118500156.ch2.

Siomi, M. C., Sato, K., Pezic, D., and Aravin, A. A. PIWI-interacting small RNAs: the vanguard of genome defence. *Nature Reviews Molecular Cell Biology*, 12(4):246–258, 2011. doi: 10.1038/nrm3089.

Slotkin, R. K. and Martienssen, R. Transposable elements and the epigenetic regulation of the genome. *Nature Reviews Genetics*, 8(4):272–285, 2007. doi: 10.1038/nrg2072.

Startek, M., Le Rouzic, A., Capy, P., Grzebelus, D., and Gambin, A. Genomic parasites or symbionts? Modeling the effects of environmental pressure on transposition activity in asexual populations. *Theoretical Population Biology*, 90:145–151, 2013. doi: 10.1016/j.tpb.2013.07.004.

Suh, A. Genome size evolution: Small transposons with large consequences. *Current Biology*, 29(7): R241–R243, 2019. doi: 10.1016/j.cub.2019.02.032.

Suh, D., Choi, E., Yamaziki, T., and Harada, K. Studies on the transposition rates of mobile genetic elements in a natural population of *Drosophila melanogaster*. *Molecular Biology and Evolution*, September 1995. doi: 10.1093/oxfordjournals.molbev.a040253.

Tomar, S. S., Hua-Van, A., and Le Rouzic, A. A population genetics theory for piRNA-regulated transposable elements. *Theoretical Population Biology*, 150:1–13, 2023. doi: 10.1016/j.tpb.2023.02.001.

Tubio, J. M., Li, Y., Ju, Y. S., Martincorena, I., Cooke, S. L., Tojo, M., Gundem, G., Pipinikas, C. P., Zamora, J., Raine, K., et al. Extensive transduction of nonrepetitive DNA mediated by L1 retrotransposition in cancer genomes. *Science*, 345(6196), 2014. doi: 10.1126/science.1251343.

van Kampen, N. G. *Stochastic Processes in Physics and Chemistry*. Elsevier, 2007. doi: 10.1016/b978-0-444-52965-7.x5000-4.

Venner, S., Feschotte, C., and Bimont, C. Dynamics of transposable elements: towards a community ecology of the genome. *Trends in Genetics*, 25(7):317–323, 2009. doi: 10.1016/j.tig.2009.05.003.

Wagstaff, B. J., Hedges, D. J., Derbes, R. S., Campos Sanchez, R., Chiaromonte, F., Makova, K. D., and Roy-Engel, A. M. Rescuing Alu: Recovery of *New* Inserts Shows LINE-1 Preserves Alu Activity through A-Tail Expansion. *PLoS Genetics*, 8(8):e1002842, 2012. doi: 10.1371/journal.pgen.1002842.

Wei, W., Gilbert, N., Ooi, S. L., Lawler, J. F., Ostertag, E. M., Kazazian, H. H., Boeke, J. D., and Moran, J. V. Human L1 retrotransposition: *cis* preference versus *trans* complementation. *Molecular and Cellular Biology*, 21(4):1429–1439, 2001. doi: 10.1128/mcb.21.4.1429-1439.2001.

Werren, J. H. Selfish genetic elements, genetic conflict, and evolutionary innovation. *Proceedings of the National Academy of Sciences*, 108:10863–10870, 2011. doi: 10.1073/pnas.1102343108.

Wicker, T., Stritt, C., Sotiropoulos, A. G., Poretti, M., Pozniak, C., Walkowiak, S., Gundlach, H., and Stein, N. Transposable element populations shed light on the evolutionary history of wheat and the complex coevolution of autonomous and nonautonomous retrotransposons. *Advanced Genetics*, 3(1), 2021. doi: 10.1002/ggn2.202100022.

Xue, C. and Goldenfeld, N. Stochastic predator-prey dynamics of transposons in the human genome. *Physical Review Letters*, 117(20), 2016. doi: 10.1103/physrevlett.117.208101.